On heating mechanisms in LEDs based on *p*-InAsSbP/*n*-InAs(Sb)

© A.L. Zakgeim [1], S.A. Karandashev [2], A.A. Klimov [2], R.E. Kunkov [2], T.S. Lukhmyrina [2],
B.A. Matveev [2,¶], M.A. Remennyi [2], A.A. Usikova [2], A.E. Chernyakov [1]

[1] Submicron Heterostructures for Microelectronics Research and Engineering Center
of the Russian Academy of Sciences,
194021 St. Petersburg, Russia
[2] Ioffe Institute,
194021 St. Petersburg, Russia
¶ E-mail: bmat@iropt3.ioffe.ru

Three main reasons for a temperature increase in activated *p*-InAsSbP/*n*-InAs/*n*-InAsSbP and *p*-InAsSbP/*n*-InAsSb/*n*-InAs double heterostructures has been considered, contribution of nonradiative Auger recombination, electron-phonon interaction and Joule heating to diode temperature increase in single element LEDs and flip-chip diode arrays (1×3) were evaluated at forward and reverse bias using data on spatial distribution of the mid-IR radiation intensity and current-voltage characteristics.

Keywords: IR LED, IR diode array, Joule heating, Auger recombination, electron-phonon interaction.

1. Introduction

The study of current heating of semiconductor $p-n$ structures is of undoubted interest both in the creation and use of high-power switches and (traditional) LEDs, and for research and development of new approaches to heat removal from working electronic components, for example, through radiation or thermoelectric cooling [1–3]. In addition, there are a number of tasks that require analysis of the temperature distribution in multi-element devices, where the spreading of heat from a working element with a $p-n$ junction changes the conditions for the operation of neighboring elements [4–7].

For LEDs of the mid-IR range of the spectrum $(2.5-6\,\mu m)$, which have a number of important practical applications in industry, medicine and ecology, the temperature increase during the flow of direct current in structures based on narrow-band semiconductors, such as InAs, InGaAs, InAsSb, etc., has been discussed repeatedly. At the same time, in many published works, the indication of the nature of the current heating of the LEDs was not completely correct, which prevented the correct interpretation of experimental data and made it difficult to understand the features of such LEDs. So, for example, quite often only one mechanism for converting electrical energy into thermal energy is mentioned, namely, Joule heating: $P_{\text{Joule}} = I_{\text{LED}}^2 \cdot R_s$, where I_{LED} — the LED current, and R_s — the serial resistance. At the same time, often tacit ignoring of other possible reasons for the LED heating was not accompanied by quantitative estimations of the heat released and (or) the estimation of the values of R_s [8–13], and in many works the experimental I−V characteristics were not given at all [5,6,8,11].

On the other hand, an alternative approach was developed in a number of works (see, for example, [14,15]) that explains the difference in the LED heating temperature with high pumping currents solely by the difference in the rates of nonradiative recombination Auger processes in the active regions of the LED based on InGaAs and InAsSbP solid solutions. Without questioning some of the experimental results given in [14], for example, in terms of the dependence of the density of inclined dislocations on the mismatch of lattice parameters on the InAsSbP/InAs heterointerface, confirming the previously obtained similar dependence in [16], still it is necessary to note the insufficient validity of the conclusions of the work [14] regarding the true reasons for LED heating to temperatures 100 K above room temperature. So, for example, there were no measurements of the I−V characteristics and the values of R_s and, accordingly, Joule heating was not taken into account when considering the LED heating data. In addition, the difference in thermal resistance between the heat sink and the $p-n$ junction in structures based on InGaAs and InAsSbP, due to the LED design features, namely the different distance from the $p-n$ junction to the heat sink, as well as the impact of the chemical composition of the heterostructure on the nature of current spreading, noted, for example, in [10], were not mentioned and, accordingly, were not taken into account. We also mention that the used LED power supply mode (sinusoidal current with an amplitude of 300 mA) should hardly be considered safe for the normal and non-degradable functioning of the LEDs described in [14].

The third group of works mentions an additional LED current heating as a result of a low internal quantum efficiency of electroluminescence *IQE* [6], however, the

corresponding temperature increase was not explicitly considered as a result of Auger recombination of charge carriers.

And finally, fourth, the most numerous group of works, actively discusses an Auger recombination in mid-IR lasers, LED and thermophotovoltaic converters, but the issues of current heating are not considered at all (see, for example, [17–20]).

This paper provides conclusions about the ratio of the contributions of the main mechanisms of current heating to temperature increase in mid-IR LED based on double heterostructures (DH) with active layers from InAs and InAsSb emitting at wavelengths near 3.4 and 4.7 μm, respectively based on I−V characteristic analysis and the distribution of the intensity of its own radiation over the surface of the chip.

1.1. Preliminary remarks

Strictly speaking, the indication of only one process of Auger recombination of nonequilibrium carriers as the reason for LED heating, given in many of the above publications, for example, in [15], is not sufficiently exhaustive, because the process of heating a semiconductor begins with the dissipation of the energy of hot carriers, i.e., with electron-phonon interaction following the Auger recombination in time. This circumstance, as a rule, is dissembled, i.e. it is understood as a matter of course, as an integral part of the general process of non-radiative recombination. At the same time, in practice, there are cases when the heating of the active region occurs without the participation of Auger recombination, but only due to electron-phonon interaction. In our opinion, such a case is realized with the reverse bias of the $p-n$ junction with an insignificant serial resistance, i.e., when operating in the negative luminescence mode, when, according to general opinion, Auger recombination is suppressed [21]. In this connection, we fill further refer the heat released during the reverse bias ($U < 0$, $I_{LED} < 0$) as the heat caused by the electron-phonon interaction, whose power at large bias and low temperature is equal to $P_{(e-ph)} = I_{LED}(U - I_{LED}R_s) = I_{LED}U_{(p-n)}$, where I_{LED} is LED current, U is the LED bias voltage, $U_{(p-n)}$ is the voltage at $p-n$ junction, R_s is the serial LED resistance. The heat released in the active region of a forward-biased LED ($U > 0$) may also be partially related to the electron-phonon interaction, for example, in case of a high rate of Auger recombination, however, at $U > 0$, the share of one or another process in heating is not as obvious as for $U < 0$, and requires separate consideration, given below.

2. Description of samples

The samples used in the work were based on p-InAs$_x$Sb$_{0.31(1-x)}$P$_{0.69(1-x)}$(2−4μm)/n-InAs(6−7 microns)/p-InAs$_x$Sb$_{0.31(1-x)}$P$_{0.69(1-x)}$(2−3μm) epitaxial heterostructures grown on InAs(100) substrates with an electronic type of conductivity, similar to those considered

in [7], and p-InAsSbP/n-InAs$_{0.9}$Sb$_{0.1}$ heterostructures of two types, differing from each other only by the degree of doping of InAs substrates, similar to those considered in [22]. The photosensitivity spectra of p-InAsSbP/n-InAs(Sb) heterostructures measured from the n-InAs substrate and the UTK1 [23] IR microscope used to register the spatial distribution of their own near-field radiation, as well as electroluminescence (EL) spectra are shown in Fig. 1, a and b. At room temperature, samples with an active layer from InAsSb had a low EL intensity with the maximum of the spectrum, amounting to $\sim 20\%$ of the intensity in samples with an active layer from InAs, other factors being equal. The spectral characteristics of the photoresponse in Fig. 1, b in the region of short wavelengths differed greatly, which was explained by the influence of the degree of doping on the optical transmission of the substrate [22]. According to the data provided on Fig. 1, b, the intensity of EL LED with an InAsSb active layer decreased by about an order of magnitude when the sample was heated from −30 up to 100°C, which is close to the dependence obtained earlier for LED based on InAs$_{0.92}$Sb$_{0.08}$ in [24]. Nevertheless, despite the slight overlapping of the EL spectra and the photosensitivity of the IR microscope, as well as the low internal quantum efficiency in InAsSb ($IQE \ll 10\%$), we still managed to register both EL radiation and negative luminescence (NL) and their spatial distribution in a sample with a broad photoresponse spectrum (#874), which will be reported later. In the sample with a narrow photoresponse spectrum (#867), the photosignal in the IR microscope due to the EL was too small, and the IR microscope recorded only thermal radiation arising from the heating of the sample.

2.1. Samples with an InAs active layer

In the first group, the chips obtained using standard photolithography had dimensions of $0.5 \times 0.5 \times 0.1$ mm and they were flip-chip diodes with an angular triangular cathode and a broad anode based on a metal composition Cr, Ni, Au, as shown in Fig. 2, a [25].

For photocurrent measurements (I_{ph}) two individual diode chips were installed opposite each other with the minimum possible distance between them, i.e. „face to face"; in some measurements, the gap between diodes/substrates is n^+-InAs was filled with optical chalcogenide glue with refractive index $\tilde{n} = 2.4$ and thickness ≤ 0.1 mm, as shown in Fig. 2, b. Chalcogenide glue has extremely low electrical conductivity, so the chips were electrically isolated from each other, and contact (mounting) ceramic boards based on AlN provided the possibility of simultaneous and independent connection of two diodes, for example, the supply of forward bias to one of the diodes (the lower diode in Fig. 2, b) and the measurement of the I−V characteristic and I_{ph} — in the other (the upper diode in Fig. 2, b). In case of the described operating mode, a similar „double sandwich" can be considered as an „immersion optocoupler" or an
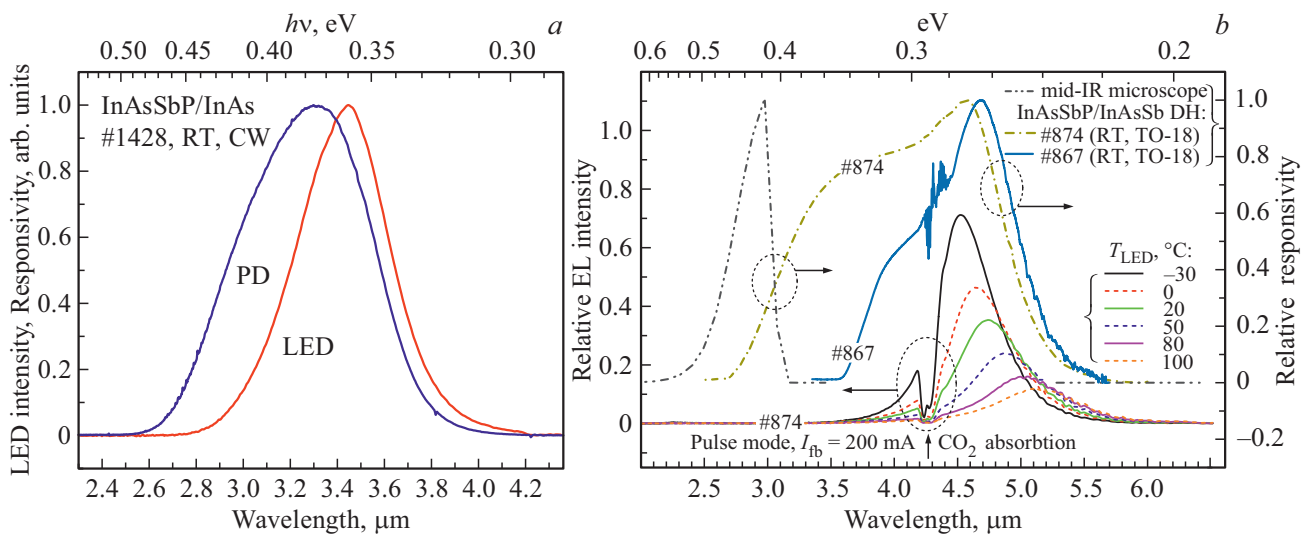
Figure 1. Spectra of EL (LED) and photosensitivity (PD) diodes based on DH $InAs_xSb_{0.31(1-x)}P_{0.69(1-x)}$/InAs at room temperature (*a*), EL spectra measured in pulsed mode at temperatures $T_{LED} = -30, 0, 20, 50, 80$ and $100°C$ (left scale), photosensitivity spectra at $20°C$ for two diodes based on DH InAsSbP/InAsSb with varying degrees of doping of the substrate *n*-InAs at room temperature, as well as the photosensitivity spectrum of the IR microscope (right scale) (*b*).

optron with a closed channel[1] with an operating wavelength near $3.4\,\mu$m.

The second group of samples from diodes with a size of 0.4×0.55 mm with a diameter of the active region $\varnothing_{mesa} = 0.2$ mm was mounted using immersion techniques in cylindrical housings with threads of the type „Sr" and provided with silicon lenses in the form of Weierstrass spheres with a diameter of $\varnothing_{lenes} = 3.5$ mm, as described in a number of publications (see, for example, [26,27]). For measurements of the light-current characteristics ($L-I$) and I_{ph}, such diodes were installed near the center of curvature of a spherical mirror with a diameter of 80 mm, which allowed collecting most of the radiation from LED on the receiving surface of the PD.

The third group of samples was a family of flat diodes 0.4×0.55 mm with round mesas with a diameter of $\varnothing_{mesa} = 45, 95, 185$ and $280\,\mu$m and wide disk anodes, the diameter of which was $\varnothing_A$ only by $20-30\,\mu$m smaller than the diameters of the mesas. Photos of the contact surface of such samples are shown in Fig. 3, *a*, in the insert to Fig. 5, as well as in [28]. At the same time, the value of the serial resistance R_s progressively increased in accordance with monotonically a decrease of the diameter of the anodes: 0.02, 0.09, 0.4 and 4 Ohms. The diodes were mounted on silicon contact boards using the flip-chip method.

Additional measurements also showed that the main part of the serial resistance of R_s diodes is related to the resistance of ohmic contacts, and not to the volume resistance of the substrate and other layers of the structure. The same applies to all other samples used in this study. At the same time, it is quite obvious that the contact

resistance is determined by the properties of the eutectic formed at the metal/semiconductor interface. For this reason, Joule heating in our case is caused by the release of heat in a material that does not have a crystal structure, i.e. in a medium to which the concepts of „phonons" and, accordingly, „electron-phonon" interaction are not strictly applicable. It is also clear that the value of the contact resistance does not depend on the direction of the current.

2.2. Samples with an active layer of InAsSb

The diodes were similar to those we described earlier in [7], i.e. they were manufactured using standard photolithography processes: each diode with a size of 0.4×0.55 mm consisted of a round mesa ($\varnothing_{mesa} = 190\,\mu$m) with a wide metal anode ($\varnothing_A = 170\,\mu$m) and a metal cathode placed on the side of the mesa. The sensor microchip with a size of 0.4×1.8 mm was a triple of the diodes described above, having a common InAs substrate, separated by etching grooves with a depth of $50\,\mu$m, located with a period of $580\,\mu$m along the long side of the chip (direction X in Fig. 3); the side surfaces of the chip were obtained by cleaving the substrate along the {110} planes. In contrast to the samples in the work [7], we mounted the chip on an AlN subcrystal board using the „flip chip" method, in which the contact-free surface of the sample, i.e., the surface of the substrate *n*-InAs faced the observer, as shown in the sample cross-section diagram in Fig. 3, *c* and photos in Fig. 3, *d*. The board with the sample was soldered to the TO-3 housing (in the terminology of the „Mars" plant (Torzhok) — „housing type 311"). Similar triples of diodes in the literature are also called „diode arrays"; within this terminology, in our study we dealt with „monolithic diode linear array 1×3". Ac-

---

[1] Other terms similar in meaning and used in the literature — „optical insulator", „microoptopair".
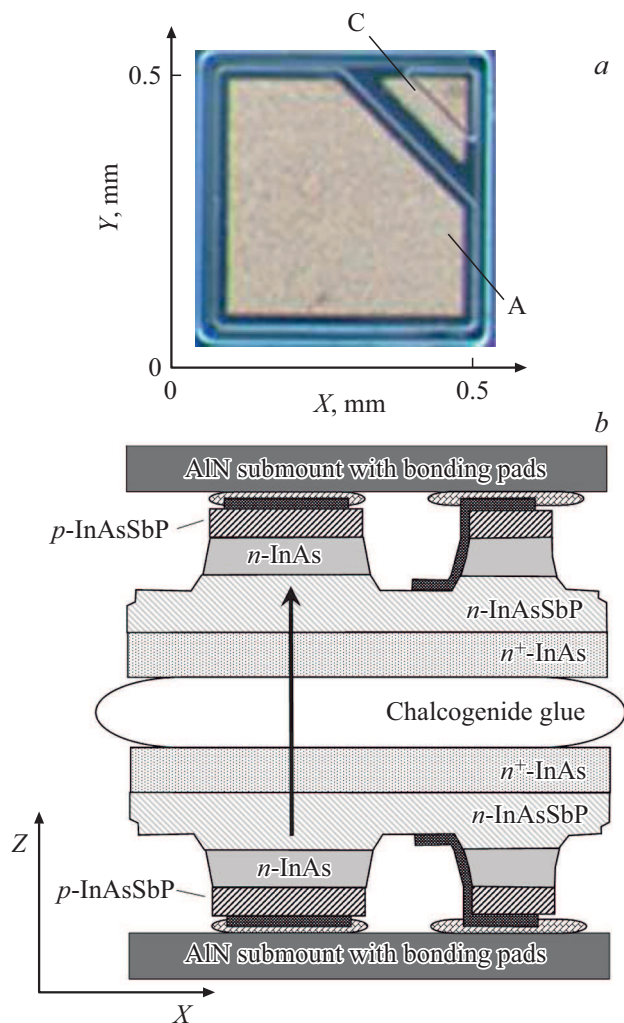
Figure 2. Photo of the chip contact surface for the first group of samples with triangular cathode („C") and wide anode („A") (see also [25]) (*a*), a diagram of a sample compiled of two identical chips with contact boards made of AlN („AlN submount with bonding pads") and an immersion layer of chalcogenide glue. The thicknesses of layers, boards and transverse dimensions are not shown in scale; the arrow shows the main direction of photon movement from LED to PD (*b*).

cording to measurements carried out on the „Thermaltester T3Ster" [29] installation, the thermal resistance between the $p-n$ transition of the central element of the array and the TO-3 housing at 300 K was $R_{th}^{300\,K} = 110$ K/W.

Fig. 3, *b* shows an IR image obtained at room temperature when applying a forward bias to the edge (on the left in Fig. 3) element of the array. It can be seen from Fig. 3, *b* that the main part of the nonequilibrium radiation comes out of the InAs substrate in the mesa region and from the adjacent edges of the chip, repeating the nature of the distribution of EL in the samples of single flat PD based on InAs [28]. The natural difference between this image and the previous one consists in a small splash caused by the reflection of a part of the EL from the inner surface of the
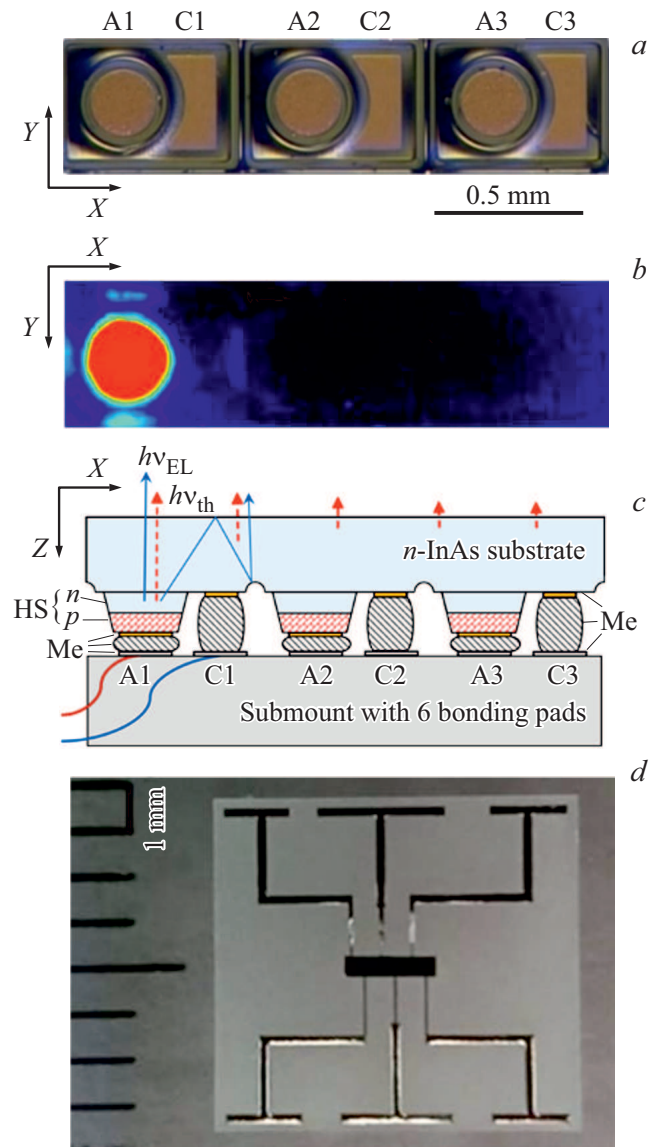

Figure 3. Photo of the epitaxial side of the chip (plane (100)) with ohmic contacts and separation grooves (*a*). IR image of the chip (1×3) from the side of the transparent substrate when the edge diode is activated ($0°$C, $I_{fb} = 50$ mA) (left element, contacts $A1, C1$) (*b*). Diagram of the longitudinal section of the chip (plane XZ, (011)) mounted on a circuit board with 6 conductors for connecting elements (Submount with 6 bonding pads), where HS — heterostructure, Me — metals (sputtered in vacuum contacts, solders), $h\nu_{EL}$ — photons born during radiative recombination of nonequilibrium charge carriers (see also solid arrows), $h\nu_{th}$ — photons born during thermal vibrations of atoms (see also dotted arrows), n-InAs substrate — indium arsenide substrate with electronic conductivity type, A1, A2, A3 — anodes, C1, C2, C3 — cathodes. n — epitaxial layers with electronic type of conductivity, p — epitaxial layers with hole type of conductivity, X — axis along the long side of the sample, axis Z — direction of epitaxial growth of DH (direction [100]). The curved lines conventionally show the wires connecting the diode to an external bias source. The diagram is not to scale (*c*). Photo of a (1×3) chip mounted on an AlN contact board with a size of 7.1×7.1 mm. The distance between the horizontal marks to the left of the board corresponds to 1 mm (*d*).
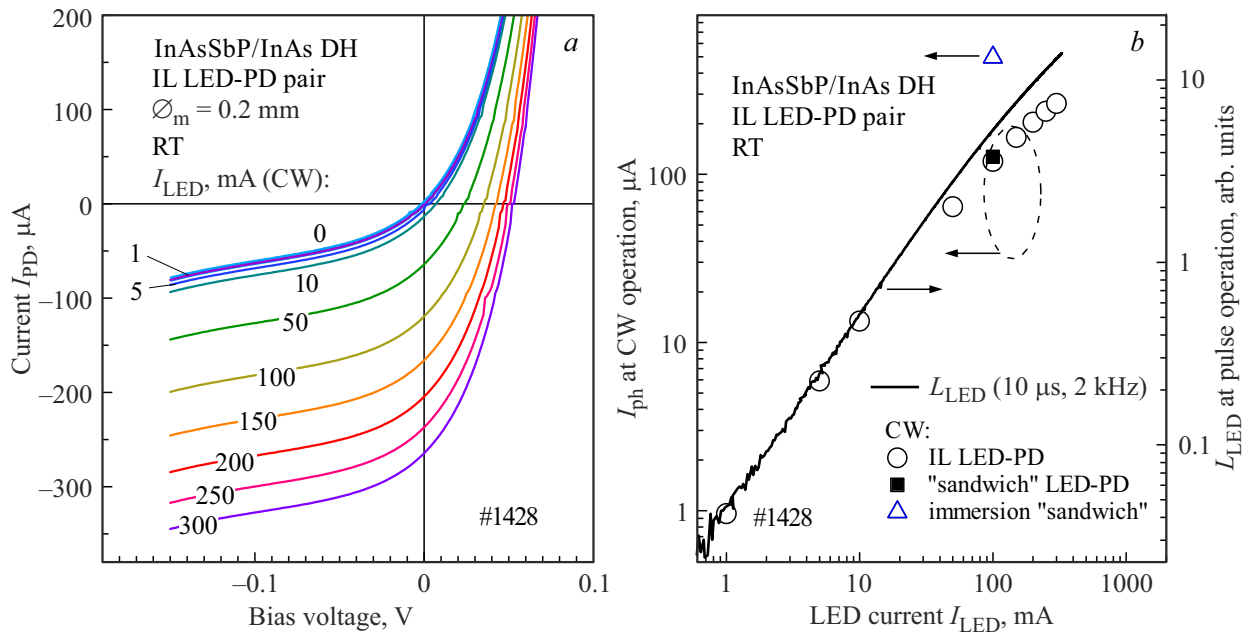
Figure 4. PD I−V characteristic as part of a discrete optocoupler with immersion lenses with LED pumping currents: 0, 1, 5, 10, 50, 100, 200 and 300 mA (*a*), the values of the photocurrent in an optocoupler consisting of discrete immersion LED and PD (circles), in an optocoupler of flat diodes with an air gap between LED and PD (squares) and an optocoupler with a filled gap between LED and PD (triangle), as well as *L*−*I* dependence for pulsed power supply (solid curve) (*b*).

dividing groove, schematically shown by the „polyline" solid arrow in the section diagram in Fig. 3, *c*. The dotted arrows in Fig. 3, *c* indicate the outputs of nonequilibrium thermal radiation from the substrate generated by heat transmitted due to vibrations of the InAs lattice (thermal conductivity). The thermal radiation was much weaker than EL under the conditions of this measurement (0°C, $I_{fb} = 50$ mA).

3. Measurement results and discussion

Fig. 4, *a* shows the PD I−V characteristic as part of an optopair with immersion lenses at various LED pumping currents. The form of the curves in Fig. 4, *a* is completely similar to those obtained earlier for a pair of PD from InAs — LED from a solid solution of InGaAs [26] with the only difference that in our case the value of the cutoff of the I−V characteristic on the ordinate axis, i.e., the value of the photocurrent I_{ph}, increased by more than 3 times compared to the previously published value. The values of I_{ph} obtained from the data in Fig. 4, *a*, as well as the values of I_{ph} for the „optron" (Fig. 2, *b*) with air gap and immersion coupling are shown in Fig. 4, *b* (left scale). The radiation intensity of a single immersion LED operating in pulsed mode ($\tau = 10\,\mu$s, $f = 2$ kHz) measured using a photodetector based on a CdHgTe solid solution (right scale), is also presented there.

As can be seen from the data shown in Fig. 4, *b*, with an increase in the pumping current, the almost linear dependence of I_{ph} on the LED current (I_{LED}) at its small values is replaced by a sublinear dependence I_{ph}

(I_{LED}), which is naturally associated with a drop in the internal quantum efficiency (IQE) of the LED. The specified decrease in IQE is most often described using the so-called ABC model as follows:

$$IQE = \frac{Bn_{inj}}{A + Bn_{inj} + Cn_{inj}^2}, \qquad (1)$$

where A, B, C are coefficients corresponding to the Shockley-Reed-Hall recombination mechanism, radiative and nonradiative Auger recombination, respectively, and n_{inj} is a concentration of injected electrons. The set of parameters *A-B-C* allows us to calculate the invariant $Q = B/(A \cdot C)^{1/2}$, which is a fundamental characteristic of the LED and allows us to determine the maximum value of $IQE_{max} = Q/(Q + 2)$ [30,31]. In our case, it is difficult to calculate the invariant Q, because it is not possible to find the parameter A, since in the experimental dependencies L−I (in Fig. 4, *b*), unlike the data in [17,19,30,31] at low currents, we do not detect a pronounced superlinear region in which Shockley-Reed-Hall recombination prevails and where $A \cdot n_{inj} > B \cdot n_{inj}^2 > C \cdot n_{inj}^3$. In addition, the difference in the slopes of the L−I dependencies for continuous and pulsed power supply in the region of high currents indicates the existence of thermal heating of the LED, which is not taken into account in any way in the ratio (1). In addition, as rightly noted in [32], the *ABC* model does not take into account the peculiarities of current spreading and heat transfer in specific LED.

In this regard, a more convenient way for us to estimate IQE is a direct measurement of the radiation power of the

LED (P_{output}) using a pre-calibrated photodetector, taking into account possible losses on the path of photons from the $p-n$ junction of the LED to the receiving area of the photodetector. At the same time, it is clear that the most reliable data can be obtained in LED-PD pairs with the lowest uncertainty in the magnitude of possible optical losses. These include pairs from the first group of samples (see Fig. 2, b); in their case the PD current sensitivity was previously measured (before assembling the optocoupler into a single unit) using a Blackbody model with a temperature of 300°C, with respect to which it could be assumed that most of the radiation released from the LED is absorbed in the PD located in the immediate vicinity.

The value obtained in the experiment $I_{ph} = 127 \, \mu A$ ($I_{LED} = 100 \, mA$) for an optocoupler without immersion coupling can be used to estimate the total optical power of radiation from the LED (P_{output}), by numerically solving the equation

$$P_{output} = \frac{I_{ph}}{S_{\lambda \, max}} \frac{\int L(\lambda) d\lambda}{\int S_I^*(\lambda) L(\lambda) d\lambda}, \qquad (2)$$

where I_{ph} — photocurrent [A], $S_I^*(\lambda)$ — relative current photosensitivity FD, $S_{\lambda \, max}$ — current photosensitivity at the maximum of the spectrum [A/W], $L(\lambda)$ — LED radiation spectrum in relative units. For $S_{\lambda \, max} = 1 \, A/W$ we get the solution of the equation (2): $P_{output} = 176 \, mW$ (1.76 mW/A). Derived from the equation (2) the value of the optical power of the LED is close to the power of the LED based on the DH $InAs_x Sb_{0.31(1-x)} P_{0.69(1-x)}/InAs$ equipped with an immersion lens [33], and is 4 times higher than the values for a LED with a wavelength near $\lambda = 3.5 \, \mu m$ based on InSb/InAlSb quantum wells [34] having the largest IQE (10%, $I_{LED} = 100 \, mA$, $P_{output} = 41 \, \mu W$) among the LED considered in the review [19]. Here we deliberately do not provide a comparison with some „record" ($P_{output} \gg 1 \, mW$) LED power values given in several of publications, because they seem overestimated to use: most of them were not mentioned later by the authors of „records", in particular, in reviews of achievements in the creation of effective mid-IR LED [19].

Low power of the flat (without immersion lenses) LEDs are usually associated with the combined effect of the total internal reflection of radiation from the semiconductor/air interface and a low value of the internal quantum efficiency ($IQE \ll 1$). Indeed, most of the photons born near the $p-n$ junction at the forward bias of the LED are reflected from the semiconductor/air interface and redirected back to the $p-n$ junction, where, due to the large thickness of the active layer, most of these photons will be absorbed, in this case they will be absorbed in the layer n-InAs[2]. Electron-hole pairs generated during this absorption can re-create photons moving towards the semiconductor/air interface. But the probability of such a process is low, and it is clear that at $IQE \ll 1$ such „re-emitted" photons

will not make a noticeable contribution to the output power of the LED. The situation may change dramatically if the conditions at the interface of the surface on which the complete EL internal reflection occurs change. According to the data in [30], the use of an immersion optically dense coating material of spherical shape $\tilde{n} = 2.4$ should result in a $\sim$ 6-fold increase of the external quantum efficiency (EQE) relative to a flat LED; in our case (see the data in Fig. 4, b) the increase in I_{ph} and, accordingly, the radiation power reaching the active region of the PD after filling the air gap with chalcogenide glass ($\tilde{n} = 2.4$) turned out to be somewhat more modest, namely it was $\sim$ 4 times (0.5 mA/0.127 mA = 3.9 at $I_{LED} = 100 \, mA$).

Considering the radiation to be monochromatic $h\nu = 0.354 \, eV$, extraction efficiency ($\gamma = EQE/IQE$) from a flat LED to be equal to $\gamma = 0.02$, and the injection efficiency to be equal to 1, we obtain for an external quantum output $EQE_{300 \, K} = P_{output} \cdot q/(Ih\nu)$ $= 5 \cdot 10^{-3}$ with the corresponding value $IQE_{300 \, K} = 0.25$. Despite the fact that the specified value slightly exceeds the largest $IQE_{300 \, K}$ from published in the literature [35], we are not inclined to claim to obtain a record high value of $IQE_{300 \, K}$ for mid-IR LEDs, because we obtained the value of $IQE_{300 \, K}$ under many assumptions, for example, under the assumption that the walls of the mesa did not participate in the increase in the proportion of radiation coming out of the LED [36]. In this regard, it seems to us somewhat overstated. In addition, as in the examples discussed in [36], there is a discrepancy between the value of $IQE_{300 \, K}$ with a simple empirical estimate taking into account the temperature dependence of EL/EQE for the interval $77-300 \, K$, obtained experimentally, namely taking into account that

$$IQE_{300 \, K} \simeq IQE_{77 \, K}/\xi_{300 \, K}^{77 \, K}, \qquad (3)$$

where $IQE_{77 \, K} = 1$, and $\xi_{300 \, K}^{77 \, K} = (EQE_{77 \, K}/EQE_{300 \, K})$ $= (P_{LED, 77 \, K}/P_{LED, 300 \, K})$ — EL[3] temperature quenching coefficient. According to the data given in [25], the coefficient of temperature quenching in similar DHs with a removed substrate is $\xi_{300 \, K}^{77 \, K} \sim 20$,[4] therefore, the data for $IQE_{77 \, K}$ and $IQE_{300 \, K}$ do not agree with each other ($IQE_{77 \, K} \ll IQE_{300 \, K}\xi_{300 \, K}^{77 \, K}$). Taking into account the change in the transmission of the substrate [25] with a decrease in temperature, the expected radiation output coefficient γ at 77 K increases slightly, but the discrepancy determined by the ratios (2) and (3) values will be maintained. Despite the fact that the reason for these discrepancies requires a separate study, the specified estimate for $IQE_{300 \, K}$ allows us drawing conclusions about the nature of the heating of the LED, given below.

The low value of $IQE_{300 \, K}$ ($\sim$ 0.25), as well as the smallness of the angle of total internal reflection in an optically

---

[2] Electrical contacts are rarely ideal, so they can also absorb some of the EL radiation.

[3] Ratio (3) doesn't not take into account the temperature dependence of the radiation-extraction efficiency γ and injection efficiency.

[4] In most cases known from the literature the values of $\xi_{300 \, K}^{77 \, K}$ for InAs-based LEDs are in the range from 10 to 30 (see, for example, [36]).
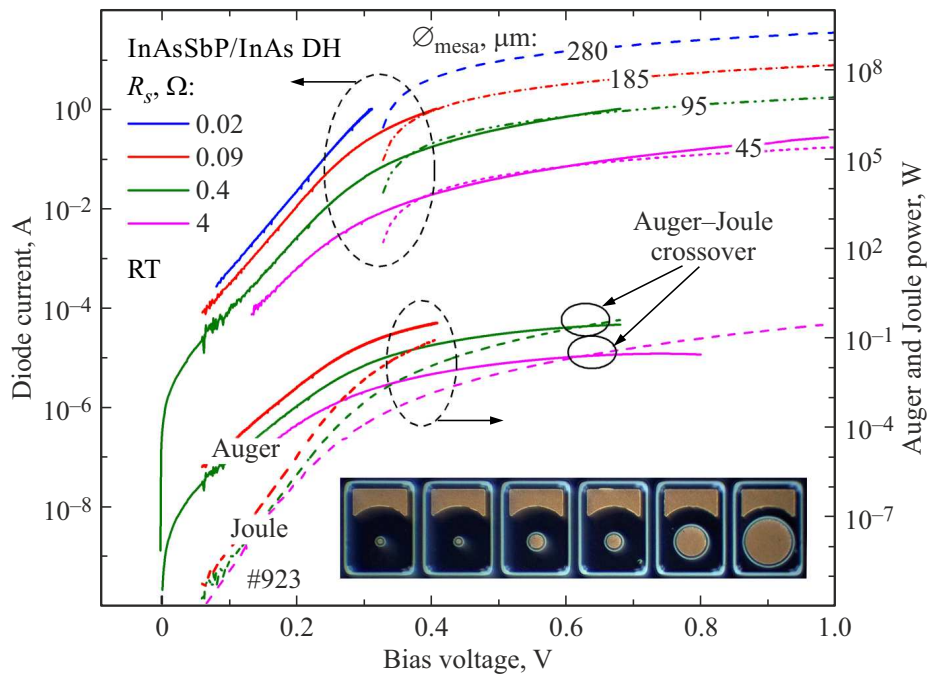
Figure 5. Left scale — I−V characteristics of four diodes with diameters of active regions $\varnothing_{\text{mesa}}$ = 280, 185, 95 and 45 μm (solid curves), function values $I = (U - 0.32)/R_s$ for R_s = 0.02, 0.09, 0.4 and 4 Ohms (dotted curves). Right scale — thermal capacities $P_{\text{Auger}} = I_{\text{LEAD}}(U\text{-}I_{\text{LED}}R_s)$ (Auger, solid curves) and $P_{\text{Joule}} = R_s I_{\text{LED}}^2$ (Joule, dotted curves). On the insert — a photo of the contact surface of diodes that differ from each other in the mesa and contact size.
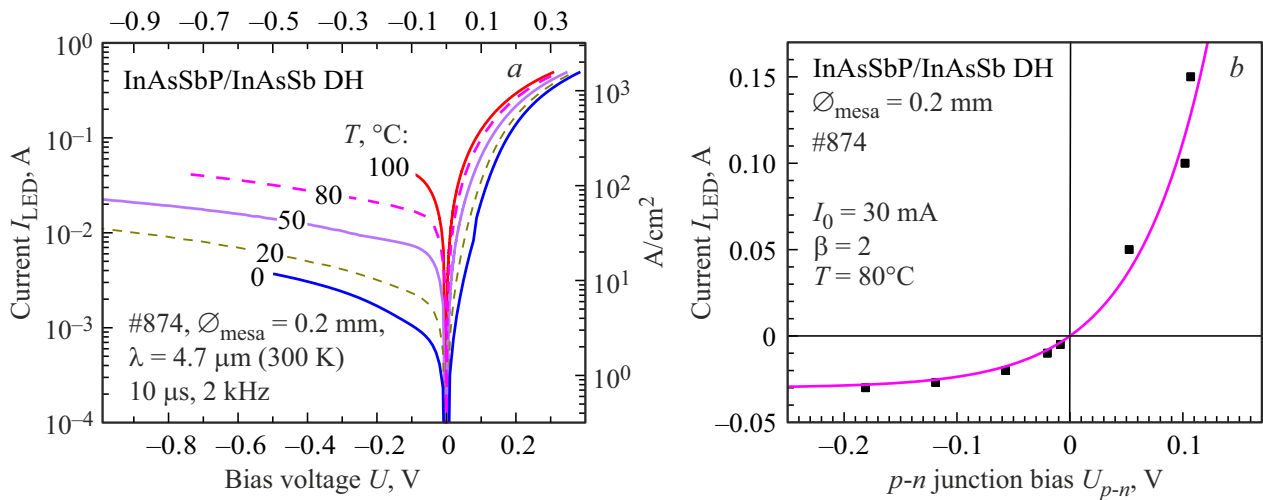

Figure 6. I−V characteristics of the diode element of the array 1×3 with an active layer of InAsSb at temperatures 0, 20, 50, 80 and 100°C with pulsed power supply (*a*), the dependence of current on voltage at $p-n$ junction $U_{p-n} = U - I_{\text{LED}}R_s$, where R_s is the value of the serial resistance determined at the linear section of the I−V characteristics at $T = 80$°C and continuous measurement mode. Solid line — function $I_{\text{LED}} = 0.03(e^{qU_{p-n}/2kT} - 1)$, [A], where k — Boltzmann constant, q — electron charge, T — temperature [K] (*b*).

dense semiconductor LED ($\tilde{n} = 3.5$) allow us to assume that at $U > 0$ almost all the electrical power supplied to the $p-n$ junction passes into „Auger power", which can be represented as $P_{\text{Auger}} \simeq P_{(\text{e}-\text{ph})} = I_{\text{LED}}(U - I_{\text{LED}}R_s)$, where U — the total voltage on the diode, R_s — its serial resistance. It is quite obvious that depending on the values of R_s and the power modes, different ratios between

Auger and Joule heat can be observed. The difference in these parameters is not difficult to detect, for example, by measuring LED samples made of the same epitaxial structure, but with different contact areas and mesas. These are the samples from the third group in our case.

Figure 5 shows the I−V chatacteristic of flip-chip diodes with different mesa diameters $\varnothing_{\text{mesa}}$ and values of R_s. As
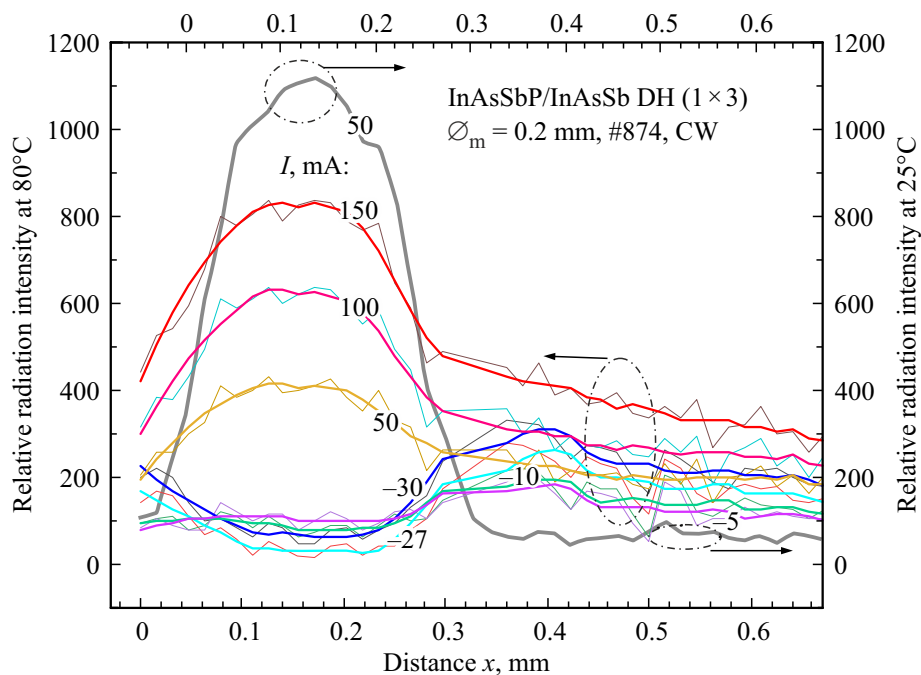
Figure 7. Distribution of the intensity of nonequilibrium intrinsic radiation in the sample at 25°C (forward current 50 mA, right scale) and at 80°C at several values of forward and reverse current in the extreme element of the array 1×3 (left scale). A slight difference in the spatial arrangement of the EL maxima at 25°C and at 80°C is caused by thermal deformations during operation of the heater (thermostat). The axis X is shifted relative to the same axes in Fig. 3.

can be seen from the data in Fig. 5, the transition from the exponential to the linear section of the I−V chatacteristic begins with biases close to $E_g/q = 0.35$ V. For diodes with a mesa diameter $\varnothing_{\mathrm{mesa}} = 45$ and $95\,\mu$m, the equality of the heat power released at the serial resistance P_{Joule} and as a result of non-radiative Auger recombination P_{Auger}, occurs at bias voltages ~ 0.65 V and currents of > 200 mA. For diodes with a larger mesa diameter (185 and 280 μm), Joule heating is secondary to „Auger heating" at reasonable values of currents ($I_{\mathrm{LED}} < 1$ A), which do not lead to catastrophic destruction/breakdown of the diode.

Fig. 6, a shows the I−V characteristic of the edge diode of the array (1×3) at several temperatures and the dependence of current on voltage at the $p-n$ junction U_{p-n} at 80°C. In the same place, in Fig. 6, b, the calculated dependence of current on voltage is given, determined by the modified Shockley formula for the passage of current caused by generation-recombination in the bulk charge layer (the current-voltage curve ideality factor $\beta = 2$), with a saturation current $I_0 = 30$ mA.

As can be seen from Fig. 7, the intensity distribution at forward current peaks in the mesa region and gradually decreases with distance from it; an increase in current is accompanied by a monotonous increase of intensity, which reflects both an increase of the intensity of the EL and an increase of thermal radiation due to an increase of the temperature of the active region of the diode. At room temperature, the contribution of EL to the radiation intensity recorded by an IR microscope sharply declines at a distance

from the mesa, reflecting unfavorable conditions for the propagation of EL radiation along the sample, mainly due to the absorption of radiation in the neighboring (middle) diode. It is possible to distinguish only a small „burst" of radiation at $x = 0.5$ mm, associated with the above-mentioned reflection from the walls of the separating groove (see Fig. 3, c), marked with a dotted circle at the bottom of Fig. 7 and a faint light strip on the IR image in Fig. 3, b.

For reverse bias, the nature of the current dependence of the intensity in the mesa region is non-monotonic: a decrease of the intensity at low reverse currents, corresponding to an increase of the power of NL, is replaced by an increase of the intensity of radiation at high currents, reflecting the saturation of the power of NL in case of large bias. Some details of these dependencies are shown in Fig. 8, where the values of the radiation intensities in two characteristic areas of the chip are provided: 1) in the region conjugate to the central part of the mesa ($x = 0.16$ mm), and 2) in the region away from the mesa, i.e., in the region of weak EL radiation ($x = 0.45$ and 0.6 mm) in depending on the pump current module ($|I_{\mathrm{LED}}|$). The narrow range of values $|I_{\mathrm{LED}}|$ at $U_{p-n} < 0$ with a sharp change of the intensity both near the center of the mesa and at a distance from it calls attention to itself. It is clear that such a sharp change can only be caused by a change in temperature, since the intensity dependences of both EL and NL on the current are smooth. Based on the previously determined value of thermal resistance (see above), the temperature change (i.e. temperature „step") of the active region (mesa)
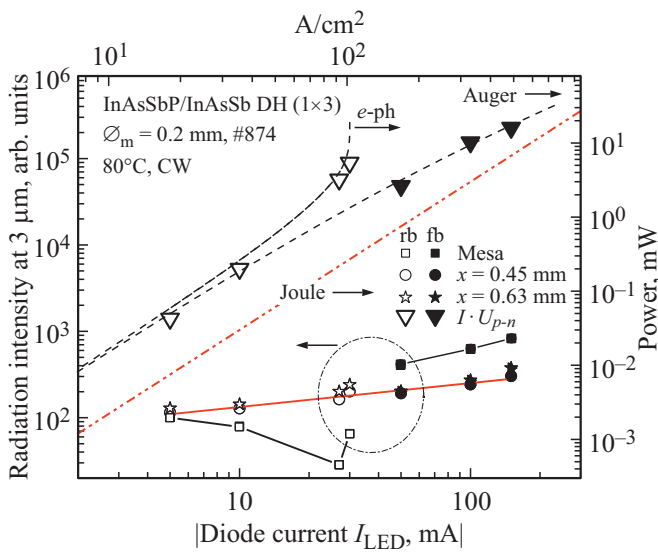
Figure 8. The dependence of the radiation intensity in the mesa region (squares) and away from it (circles and stars) on the current modulus in the extreme element of the diode ruler 1×3 (left scale) and the dependence of the power allocated at the serial resistance $R_s = 0.3$ Ohms (red dashed dotted line), with electron-phonon interaction (dotted black curve and unpainted triangles) and non-radiative Auger recombination (dotted black curve, shaded triangles) (right scale). The filled characters refer to the data for the forward bias, „empty" characters refer to the reverse bias.

with an increase in the reverse current from 27 to 30 mA at 80°C was $\Delta T_{\#874} = R_{\mathrm{th}}^{300\,\mathrm{K}} \Delta P = 0.3$ K. The temperature change with the same values of the product of $U_{p-n} \times I_{\mathrm{LED}}$, obtained using the values of the radiation intensities from the region above the mesa and the previously obtained IR calibration of the microscope, was $\Delta T_{\#867} = 0.5$ K for the mesa region in a sample with an opaque substrate (#867) when heated by direct current. The differences in the properties of structures and their assembly conditions, in contrast to the obtained values of ΔT, can be considered insignificant if the temperature dependence of the thermal resistance $R_{\mathrm{th}}^{300\,\mathrm{K}}(T)$ is ignored.

A sharp change of the temperature with a relatively small change of current is unlikely to be associated with Joule heating, which has a smooth, quadratic dependence on current. The heating involving electron-phonon interaction in the narrow-band active layer InAsSb is a different matter, for which *IQE* is no more than units of percent at room temperature [19] and decreases sharply at elevated temperatures (Fig. 1, *b*, [24]). Taking into account the coordinates proposed in Fig. 8, it is not difficult to detect a narrow range of current values in which the product of current and voltage at the $p-n$ junction experiences a sharp increase, and this region coincides with the region of the „anomalous" change in the intensity of thermal radiation, i.e., the temperature of the sample. It is possible to add that the Joule heating power is significantly inferior to the values of $I_{\mathrm{LED}} U_{p-n}$ (see the data in Fig. 8).

4. Conclusion

It follows from the data presented in the paper that the predominance of heating due to non-radiative Auger recombination over other types of thermal heating in a LED with a low radiation output coefficient is not something taken for granted, and therefore, when formulating the reasons for heating, it is necessary to make estimates of the internal quantum efficiency, the magnitude of the serial resistance of a particular LED and take into account the geometric features of the LED, including the resistance of its individual parts, such as the anode and cathode. In mid-IR diodes with low serial resistance operating with a reverse bias, i.e. in the negative luminescence mode, the electron-phonon interaction process should be considered dominant for heating the diode. With forward bias, such diodes can also be considered as „heating elements", used, for example, to create semiconductor sensors that are convenient for measuring temperature. The use of these features is justified, for example, when measuring the disturbed total internal reflection using miniature ATR sensors, for which it is much more convenient to stabilize the temperature of the elements above the environment using forward-biased LED (i.e. Auger heaters) than to overload the sensor design with devices such as Peltier elements [7].

Conflict of interest

The authors declare that they have no conflict of interest.

References

[1] P. Santhanam, D. Huang, R.J. Ram, M.A. Remennyi, B.A. Matveev. Appl. Phys. Lett., **103** (19), 183513 (2013).

[2] Jin Xue, Yuji Zhao, Sang-Ho Oh, W.F. Herrington, J.S. Speck, S.P. DenBaars, Shuji Nakamura, R.J. Ram. Appl. Phys. Lett., **107**, 121109 (2015).

[3] L. Zhu, A. Fiorino, D. Thompson., R. Mittapally, E. Meyhofer, P. Reddy. Nature, **566**, 239 (2019).

[4] B.K. Tanner, A. Danilewsky, P.J. McNally. J. Appl. Cryst., **55**, 1139 (2022).

[5] V. Malyutenko, A. Zinovchuk. Proc. SPIE, **6368**, 63680D (2006).

[6] J.V. Lawler, J. Currano. Proc. SPIE, **6942**, Art. no. 69420E-1 (2008).

[7] S.A. Karandashev, T.S. Lukhmyrina, B.A. Matveev, M.A. Remennyi, A.A. Usikova. Phys. Status Solidi A, **219** (2), 2100456 (2022)

[8] A.P. Astakhova, A.S. Golovin, N.D. Ilyinskaya, K.V. Kalinina, S.S. Kizhaev, O.Yu. Serebrennikova, N.D. Stoyanov, Zs.J. Horvath, Yu.P. Yakovlev. FTP, **44** (2), 278 (2010). (in Russian).

[9] V.K. Malyutenko. Mater. Res. Soc. Symp. Proc., **744**, M4.10.1 (2002).

[10] V.K. Malyutenko, A.V. Zinovchuk, O.Yu. Malyutenko. Semicond. Sci. Technol., **23** (8), 085004 (2008).

[11] A.A. Popov, M.V. Stepanov, V.V. Sherstnev, Yu.P. Yakovlev. Pisma ZhETF **15**, 34 (1998). (in Russian).

[12] A. Krier, V.V. Sherstnev. J. Phys. D: Appl. Phys., **34**, 428 (2001).

[13] C.A. Karandashev, T.S. Luhmyrina, B.A. Matveev, M.A. Remenny, A.A. Usikova. Opt. i spektr., *129* (9), 1193 (2021). (in Russian).

[14] G.A. Sukach, A.B. Bogoslovskaya, P.F. Oleksenko, Yu.Yu. Bilynets, V.N. Kabacij. Infr. Phys. Technol., **41**, 299 (2000).

[15] G.A. Sukach, P.F. Oleksenko, A.B. Bogoslovskaya, Yu.Yu. Bilinets, V.N. Kabatsky. ZhTF, **67** (9), 68 (1997). (in Russian).

[16] S.G. Konnikov, B.A. Matveev, T.B. Popova, N.M. Stus, G.N. Talalakin, V.E. Umansky. Sov. Phys. Solid State, **28**, *3*, 439 (1986).

[17] A. Krier, M. Yin, V. Smirnov, P. Batty, P.J. Carrington, V. Solovev, V. Sherstnev. Phys. Status Solidi A, **205** (1), 129 (2008).

[18] A. Semakova, N.L. Bazhenov, K.D. Mynbaev. J. Phys.: Conf. Ser., **1038**, 012097 (2018).

[19] A. Krier, E. Repiso, F. Al-Saymari, P.J. Carrington, A.R.J. Marshall, L. Qi, S.E. Krier, K.J. Lulla, M. Steer, C. MacGregor, C.A. Broderick, R. Arkani, E. O'Reilly, M. Sorel, S.I. Molina, M. De La Mata. *Mid-infrared light-emitting diodes*. In: *Mid-infrared Optoelectronics. Materials, Devices, and Application* (Woodhead Publishing Series in Electronic and Optical Mater., 2020) p. 59.

[20] G.P. Forcade, C.E. Valdivia, S. Molesky, S. Lu, A.W. Rodriguez, J.J. Krich, R. St-Gelais, K. Hinzer. Appl. Phys. Lett., **121** (19), 193903 (2022).

[21] V.I. Ivanov-Omsky, B.A. Matveev. FTP, **41** (3), 2570 (2007). (in Russian).

[22] P.N. Brunkov, N.D. Il'inskaya, S.A. Karandashev, A.A. Lavrov, B.A. Matveev, M.A. Remennyi, N.M. Stus', A.A. Usikova. Infr. Phys. Technol., **73**, 232 (2015).

[23] V.M. Basovkin, A.A. Gusev, A.P. Kovchavtsev, G.L. Kuryshev, A.S. Lapshin, V.G. Polovinkin. Prikl. fizika, **2**, 97 (2005). (in Russian).

[24] N.V. Zotova, N.D. Ilyinskaya, S.A. Karandashev, B.A. Matveev, M.A. Remenny, N.M. Stus. FTP, **40** (6), 717 (2006). (in Russian).

[25] S.A. Karandashev, A.A. Klimov, R.E. Kunkov, A.A. Lavrov, T.S. Lukhmyrina, B.A. Matveev, M.A. Remennyi, A.A. Usikova. J. Phys.: Conf. Ser., **410** (1), 012028 (2019).

[26] B.A. Matveev; N.V. Zotova, S.A. Karandashev, M.A. Remennyi, N.M. Stus', G.N. Talalakin. Proc. SPIE, **4650**, 173 (2002).

[27] N. Dyakonova, S.A. Karandashev, M.E. Levinshtein, B.A. Matveev, M.A. Remennyi, A.A. Usikova. Infr. Phys. Technol., **117**, 103867 (2021).

[28] A.L. Zakheim, N.D. Ilyinskaya, S.A. Karandashev, A.A. Lavrov, B.A. Matveev, M.A. Remenny, N.M. Stus, A.A. Usikova, A.E. Chernyakov. FTP, **51** (2), 269 (2017). (in Russian).

[29] Simcenter T3STER http://www.micred.com/t3ster/

[30] A.L. Zakheim. *LEDs and their application* (M., Svetotekhnika, 2021).

[31] S. Karpov. Optical Quant. Electron., **47**, 1293 (2015).

[32] V.K. Malyutenko, A.D. Podoltsev, O.Yu. Malyutenko. Jpn. J. Appl. Phys., **118**, 153105 (2015).

[33] IoffeLED www.ioffeled.com

[34] L. Meriggi, M.J. Steer, Y. Ding, I.G. Thayne, C. Macgregor, C.N. Ironside, M. Sorel. 11th Conf. on Ph. D. Research in Microelectronics and Electronics (PRIME), 29 June, Glasgow, UK, IEEE, 180 (2015).

[35] M.J. Kane, G. Braithwaite, M.T. Emeny, D. Lee, T. Martin, D.R. Wright. Appl. Phys. Lett., **76**, 943 (2000).

[36] S.A. Karandashev, B.A. Matveev, M.A. Remenny. FTP, **53** (2), 147 (2019). (in Russian).

Translated by A.Akhtyamov